Pure Ni-Based and Trimetallic Ni-Co-Fe Catalysts for the Dry Reforming of Methane: Effect of K Promoter and the Calcination Temperature

Ghazaleh Khoshroo[1] · András Sápi[1] · Imre Szenti[1] · Anastasiia Efremova[1] · Henrik Bali[1] · Kornélia B. Ábrahámné[1] · András Erdőhelyi[1] · Ákos Kukovecz[1,2] · Zoltán Kónya[1,2]

Abstract

This work investigates the effect of the Potassium promoter and the calcination temperature on the catalytic activity in the dry reforming of methane reaction and compares the performance of the Ni, Co, Fe–Al$_2$O$_3$ trimetallic catalysts with the reference Ni–Al$_2$O$_3$. Although higher activity was achieved with the Ni–Al$_2$O$_3$, trimetallic catalysts resulted in a more favorable CO/H$_2$ ratio and considerably better coke resistance. Higher calcination temperature led to the increase in coke formation which caused the sintering of the catalysts. Promoting samples with 0.5%K in order to improve the coke formation resistance, reduced the catalytic activity.

Graphical Abstract
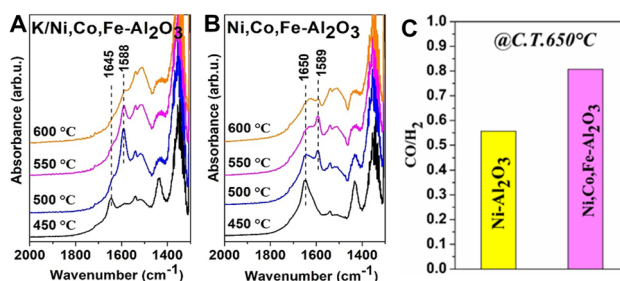
1 Introduction

In recent years, the rise in population and associated industrial needs have resulted in significant growth in the consumption of fossil fuels which has introduced various environmental pollutants into the atmosphere. This has led to a quick increase in greenhouse gas emissions including carbon dioxide which is the main reason for global warming and climate change. Methane is another greenhouse gas that is 25 times more likely to cause global warming [1–3].

In order to reduce the emission of these two main greenhouse gases, technical methods such as capture, catalytic conversion, and sequestration have been used. Dry reforming of methane (DRM) is a complicated catalytic reforming process (Eq. 1–3) that has received much attention among other approaches [4–6].
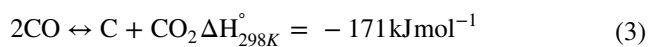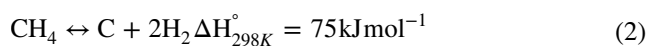
This method utilizes methane and carbon dioxide as feedstock to produce synthesis gas. The ratio of CO/H$_2$ in the final product is near to one which is suitable for Fischer–Tropsch synthesis.

$$CH_4 + CO_2 \leftrightarrow 2CO + 2H_2 \, \Delta H^{\circ}_{298K} = 247 kJ mol^{-1} \qquad (1)$$

✉ András Sápi
  sapia@chem.u-szeged.hu

[1] Interdisciplinary Excellence Center, Department of Applied and Environmental Chemistry, University of Szeged, Rerrich Béla tér 1, 6720 Szeged, Hungary

[2] MTA-SZTE Reaction Kinetics and Surface Chemistry Research Group, University of Szeged, 6720 Szeged, Hungary

$$CH_4 \leftrightarrow C + 2H_2 \; \Delta H^{\circ}_{298K} = 75 \, kJmol^{-1} \tag{2}$$

$$2CO \leftrightarrow C + CO_2 \; \Delta H^{\circ}_{298K} = -171 \, kJmol^{-1} \tag{3}$$

Based on the thermodynamic analysis, DRM is a highly endothermic reversible reaction that needs a high reaction temperature. As a result, catalysts applied in such circumstances may become deactivated because of the sintering of active metals. Moreover, during the DRM process, there are side reactions that lead to coke deposition (Eq. 2, 3) [7].

Ni-based catalysts have received a lot of attention for DRM owing to their accessibility, reasonable cost, and initial activity comparable to noble metals catalysts. However, quick deactivation and sintering of Ni due to coke formation is a big challenge [8–10]. In order to reduce catalyst coking, choosing appropriate support with mobile surface/subsurface oxygen with strong CO_2 activation ability and alloying nickel with a second metal are the two common approaches [11]. As DRM requires high temperature, oxide supports with high specific surface area and good thermal stability such as alumina are needed. Utilization of Al_2O_3 support for Ni can relieve the coke deposition because of the strong metal-support interaction and enhances the stability of the catalyst [12].

In catalyst design, the most common method is to add another metal to the catalyst as a promoter. Alkali and earth alkali metals such as K are the most popular promoters which are able to boost the catalytic performance in several different ways and can increase the resistance to coking. As the formation of coke happens on bigger Ni particles or on step-edge sites on the Ni surface, promoters prevent coke formation by blocking highly reactive sites [13–15]. In recent years, bimetallic catalysts have attracted a lot of interest as a way to enhance catalytic activity. Owing to their unique physical and chemical features that are different from of their parent metals, bimetallic catalysts can add new features including promoted activity, selectivity, and stability properties. The recent research demonstrated that Ni–Fe alloy due to its redox functionality provided by Fe, has the ability to restrain carbon formation and upgrade the metal-support interaction which causes high dispersion [16, 17]. When Co and Ni are reduced together, they have similar radii, making it easy to form an alloy within a special molar range, and thus CH_4 is activated faster. Meanwhile, Co has a high oxygen affinity, which can significantly raise the concentration of O on the catalyst surface and enhance carbon gasification [18]. Joo et al. prepared Co–Ni–Fe ternary alloy nanoparticles using topotactic exsolution on the PBMCoNi system. This resulted in the upshift of the d-band center for Co–Ni–Fe ternary alloy and promoted the activation of the CO_2 and CH_4 reactants [19].

In this study, Ni,Co,Fe–Al_2O_3 catalysts were synthesized under different calcination temperatures: 650, 750, and 850 °C and further promoted by 0.5%K. The three metals' synergetic effects and the influence of calcination temperature on catalytic activity in DRM were studied.

2 Experimental

2.1 Chemicals

Nickel (II) nitrate, Co (II) nitrate hexahydrate, Iron (III) nitrate nonahydrate, Potassium nitrate, and gamma-alumina (γ-Al_2O_3).

2.2 Synthesis of Catalysts

2.2.1 Synthesis of 3%Ni–Al_2O_3 & 3%Ni,0.5%K–Al_2O_3 particles

The support (γ-Al_2O_3, Degussa AG) was impregnated with the aqueous solution of.

$Ni(NO_3)_2 \cdot 6H_2O$ to yield a nominal 3wt% metal content. In order to produce promoted catalysts, KNO_3 was added to the aqueous solution to yield 0.5wt% of Potassium.

2.2.2 Synthesis of 1%Ni, Co, Fe–Al_2O_3 & 1%Ni, Co, Fe,0.5%K–Al_2O_3

The catalysts were prepared by the impregnation of γ-Al_2O_3 (Degussa AG) with an aqueous solution of $Ni(NO_3)_2 \cdot 6H_2O$, $Co(NO_3)_2 \cdot 6H_2O$, and $Fe(NO_3)_3 \cdot 9H_2O$ to result in 1wt% amount of each metal. For promoted analogs, an aqueous solution of KNO_3 was used to yield 0.5wt%.

All the samples were dried at 110 °C and calcined at 650,750, and 850 °C.

2.3 Catalytic Tests

Catalytic reactions were conducted in a fixed-bed continuous flow reactor. The ratio of CH_4/CO_2 in the reacting gas mixture was 1:1 and the range of reaction temperature was 450–750 °C. The loaded catalyst was 0.1 g. The reactants' flow rate was 30 ml/min. The separation and analysis of the gases was carried out with the Agilent 6890 gas chromatograph using the HP-PLOT Q column. The catalysts were oxidized at 400 °C in O_2 flow for 30 min and reduced at 600 °C under H_2 flow for 60 min in situ based on TPR results (Fig. 1) which will be discussed later.
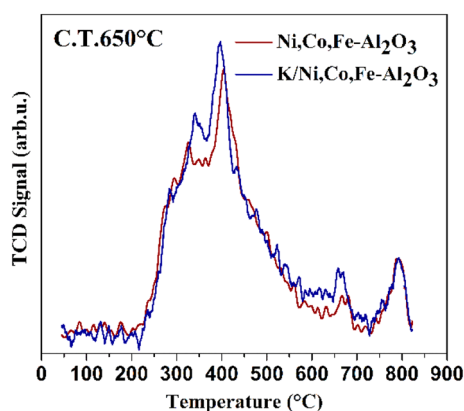
Fig. 1 H$_2$-TPR profiles of Ni,Co,Fe–Al$_2$O$_3$ and K/Ni,Co,Fe–Al$_2$O$_3$ calcined at 650 °C

2.4 Characterization of the Catalysts

The specific surface area, the pore size distribution, and the total pore volume were determined by a Quantachrome NOVA 2200 gas sorption analyzer by N$_2$ gas adsorption/desorption at − 196 °C and calculated by BET and BJH equations. Before the measurements, the samples were pretreated in a vacuum (< ∼ 0.1 mbar) at 200 °C for 2 h.

The X-ray diffraction spectra were acquired using a Rigaku MiniFlex II instrument with a Ni-filtered CuKα source in the range of 2θ = 5–100°.

The temperature-programmed reduction (TPR) and carbon dioxide temperature-programmed desorption (CO$_2$-TPD) measurements were carried out in a BELCAT-A apparatus using a reactor (quartz tube with a 9 mm outer diameter) that was externally heated. Before the measurements, the catalyst samples were treated in oxygen at 200 °C for 30 min. Thereafter, the samples were cooled in

flowing N$_2$ to room temperature. The oxidized samples were flushed with N$_2$ containing 10% H$_2$ or with CO$_2$ for 30 min, flushed with N$_2$ for 15 min, and the reactor was heated linearly at a rate of 10 °C/min from 50 °C to 800 °C in the case of TPR and to 600 °C in the case of CO$_2$-TPD. The H$_2$/CO$_2$ consumption was detected by a thermal conductivity detector (TCD). The flowing rate was 50 ml/min in all cases.

TEM images of the samples presented on a carbon-coated copper grid were provided by FEI TECNAI G2 20 X-Twin high-resolution transmission electron microscope (equipped with electron diffraction) operating at an accelerating voltage of 200 keV.

3 Results and Discussion

3.1 Catalyst Characterization

Table 1 shows the N$_2$ adsorption analysis results for all catalysts. Among trimetallic catalysts, the samples calcinated at 650 °C showed somewhat a higher specific surface area while the highest amount was demonstrated by the Ni–Al$_2$O$_3$. An increase in the calcination temperature resulted in a decrease in surface area. This may be caused by the sintering of the catalyst and subsequent particle growth [20]. In addition, promoted samples showed lower surface area.

The H$_2$-TPR measurements were performed for trimetallic catalysts and their promoted counterparts. The calcination temperature did not influence the reduction properties of the samples. TPR profiles for Ni, Co, Fe–Al$_2$O$_3$ and K/Ni, Co, Fe–Al$_2$O$_3$ (C.T:650 °C) are given in Fig. 1. Based on other studies, the reduction of alumina supported nickel-based catalysts to metallic nickel occurs at temperatures < 600 °C [21, 22]. Supporting this, our results demonstrated that the

Table 1 N$_2$ adsorption analysis results

Sample	BET surface area, m^2/g	Pore Volume, cm^3/g	Pore Size, nm
γ-Al$_2$O$_3$	101.575	0.1737	6.84153
3%Ni–Al$_2$O$_3$(C.T:650 °C)	100.924	0.3818	15.1320
3%Ni,0.5%–Al$_2$O$_3$(C.T:650 °C)	96.704	0.3282	13.5765
1%Ni, Co, Fe–Al$_2$O$_3$(C.T:650 °C)	93.939	0.4376	18.6319
1%Ni, Co, Fe,0.5%K–Al$_2$O$_3$(C.T:650)	91.676	0.3693	16.1125
3%Ni–Al$_2$O$_3$(C.T:750 °C)	93.769	0.4289	18.2972
3%Ni,0.5%K-Al$_2$O$_3$(C.T:750 °C)	92.529	0.2982	12.8909
1%Ni, Co, Fe–Al$_2$O$_3$(C.T:750 °C)	90.585	0.3519	15.5408
1%Ni, Co, Fe,0.5%K–Al$_2$O$_3$(C.T:750 °C)	91.525	0.3886	16.9823
3%Ni–Al$_2$O$_3$(C.T:850 °C)	89.767	0.4702	20.9502
3%Ni,0.5%K–Al$_2$O$_3$(C.T:850 °C)	89.767	0.4702	20.9502
1%Ni, Co,Fe–Al$_2$O$_3$(C.T:850 °C)	91.059	0.3465	15.2202
1%Ni, Co,Fe,0.5%K–Al$_2$O$_3$(C.T:850 °C)	88.760	0.3041	13.7034

600 °C pre-treatment temperature leads to the formation of the metallic phase. Peaks at ~ 700 °C, ~ 800 °C could be attributed to the reduction of metal aluminates: $Ni–Al_2O_4$, $Co–Al_2O_4$, and $Fe–Al_2O_4$ which may form as a result of the interaction of the metals with the alumina support [23, 24].

CO_2-TPD analysis was carried out to identify the number of basic sites present on the oxidized catalysts (Fig. 2). Obviously, the peak area of basic sites for the trimetallic catalyst was considerably larger after Potassium incorporation, which may greatly assist in the CO_2 adsorption during dry reforming of methane reaction.

The XRD analysis was implemented to study the composition of the samples and the phase transformation caused by the calcination. Typical reflections of trimetallic catalysts calcined at different temperatures, of their K-promoted counterparts, and of the $γ-Al_2O_3$ which was used as the support are presented in Fig. 3A. All the diffraction peaks were attributed to the crystal planes of $γ-Al_2O_3$ (JCPDS no. 29–0063) among which the (400) and

the (440) reflections had the highest intensity in accordance with other studies [25, 26]. No reflections which indicate the presence of bulk metals or their oxides were registered. However, the formation of aluminates during the calcination cannot be excluded since the reflections of MAl_2O_4, where M = Co,Ni,Fe are known to greatly overlap with those of $γ-Al_2O_3$ [27, 28]. The formation of aluminates is suggested from the H_2-TPR analysis data as well. The interaction of transition metals with the support is observed in the improved crystallinity: all trimetallic samples exhibited sharper peaks of higher intensity. At the same time, the loading of a small amount of Potassium has the opposite effect. For comparison, promoted and unpromoted $Ni–Al_2O_3$ calcined at various temperatures was also analyzed by XRD (Fig. 3B). Similar conclusions can be derived in this case as well.

Transmission electron microscopy was applied to investigate the microstructure of the prepared samples. All the samples exhibit similar textures originating from $γ-Al_2O_3$ with particles of various shapes and 10–15 nm in diameter. As an example, TEM analysis results are shown for the $Ni,Co,Fe–Al_2O_3$ sample calcined at 650 °C (Fig. 4A) and its promoted analogue (Fig. 4B). The homogeneity of morphology was assured by investigating multiple areas on the TEM grid. The ED patterns demonstrate intense reflections of (400) and (440) planes as well several weaker reflections of the $γ-Al_2O_3$. In high magnification images, lattice fringes are visible which further confirms the crystalline nature of the trimetallic catalysts in agreement with XRD results. Calculated d-spacings from HR-images agree well with theoretical values. In Fig. 4, ~ 4.92 Å d-spacing corresponds to (111) crystal plane of the fcc structure of $γ-Al_2O_3$. No significant differences in the d-spacing values after the promotion with Potassium were observed. This indicates high dispersion of Potassium.
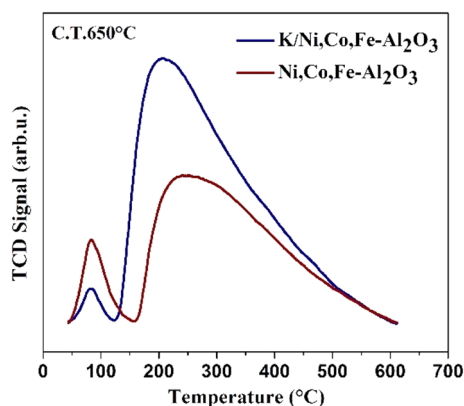

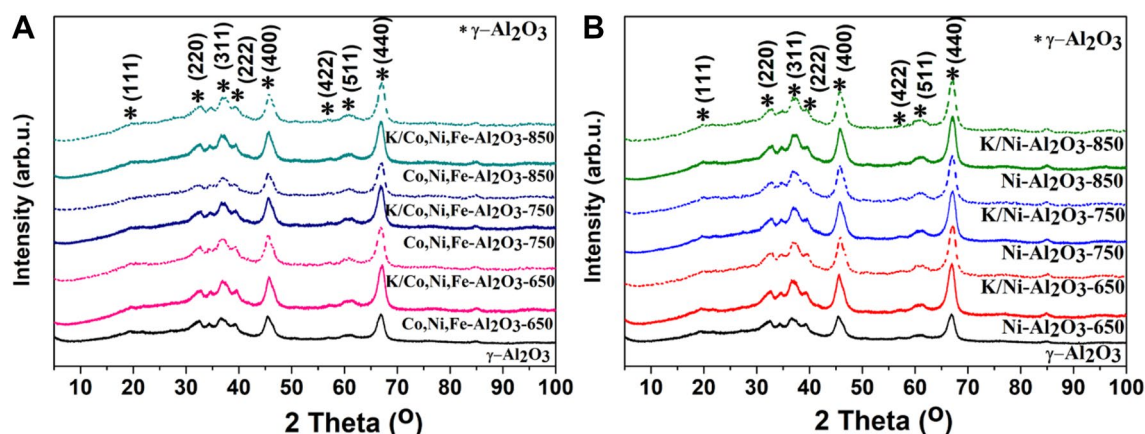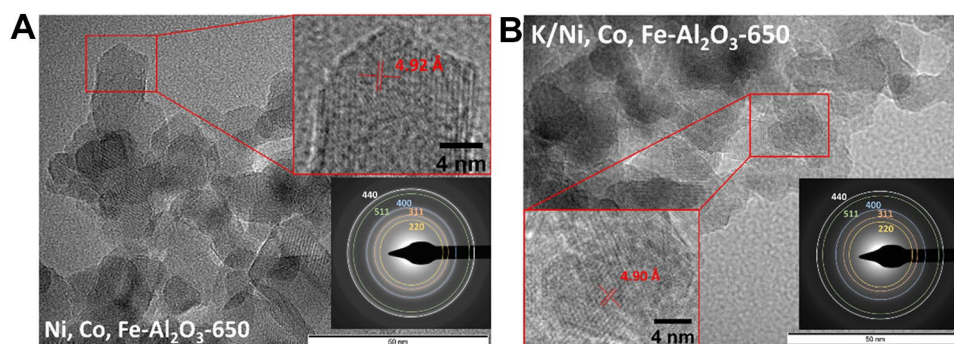**Fig. 2** CO_2-TPD curves of Ni, Co, Fe–Al_2O_3 and K/Ni, Co, Fe–Al_2O_3 calcined at 650 °C

Fig. 3 XRD patterns of the **A** $γ-Al_2O_3$, Ni,Co,Fe–Al_2O_3 as well as the K/Ni,Co,Fe–Al_2O_3 calcined at 650, 750 and 850 °C; **B** $γ-Al_2O_3$, Ni–Al_2O_3 as well as the K/Ni–Al_2O_3 calcined at 650, 750 and 850º

Fig. 4 TEM image, HR-TEM image, and ED pattern of **A** Ni,Co,Fe–Al$_2$O$_3$, and **B** K/Ni,Co,Fe–Al$_2$O$_3$ calcined at 650 °C

3.2 Catalytic Results

3.2.1 Effect of the Calcination Temperature

The catalytic activity measurements revealed that optimal calcination temperature which results in higher reactant gases conversion for both Ni-supported and trimetallic catalysts is 650 °C (Fig. 5). The decrease in catalytic activity at higher calcination temperatures is caused by the sintering which in turn results in lower dispersion and larger size of the metal particles. The formation of metal crystallites during calcination happens mostly in the first phase of heating and is hardly controllable when applying the impregnation method [29]. This limits the dispersion that can be achieved. Following soaking at the calcination temperature, the generated crystallites from decomposed precursors interact more strongly with the support [29]. With regards to the selectivity, although Ni,Co,Fe–Al$_2$O$_3$ has shown to be less active, it in turn produces more favorable CO/H$_2$ ratio which is preferable for the Fischer–Tropsch process (Fig. 5C).

3.2.2 Catalyst Deactivation

The extensive carbon deposition, which causes quick deactivation of the catalyst during operation, is one of the major

disadvantages of DRM [30, 31] Fig. 6 demonstrates the XRD results of the spent catalyst. The sharp diffraction peak $2\theta = \sim 26°$ in the case of Ni–Al$_2$O$_3$ is attributed to the (002) plane of graphite [32]. This peak is substantially lower for the Ni,Co,Fe–Al$_2$O$_3$, which indicates that the synergetic effect of trimetallic catalysts is able to decrease the coke formation during the reaction. To further confirm minimum coke deposition on the trimetallic catalyst, TPR experiments were conducted. In a typical experiment, the catalyst was kept under reaction conditions for 2 h at 750 °C. After cooling in Ar to 50 °C, the flow was switched to H$_2$, and the oven was linearly heated to 850 °C with 10 °C/min heating rate. The formation of hydrocarbons, primarily methane, was followed. Minimum amount of methane was detected.

3.2.3 Influence of the Potassium Promoter

It is well known that addition of small amount of Potassium aids in the suppression of carbon deposition [33]. Moreover, Potassium increases the catalyst basicity and thus assist in the CO$_2$ activation. 0.5%K-promoted nickel and trimetallic catalysts were prepared and tested for the dry reforming process. Compared to the unpromoted catalysts, loading of 0.5%K had a negative effect on the catalytic performance at all calcination temperatures. According to literature, the step
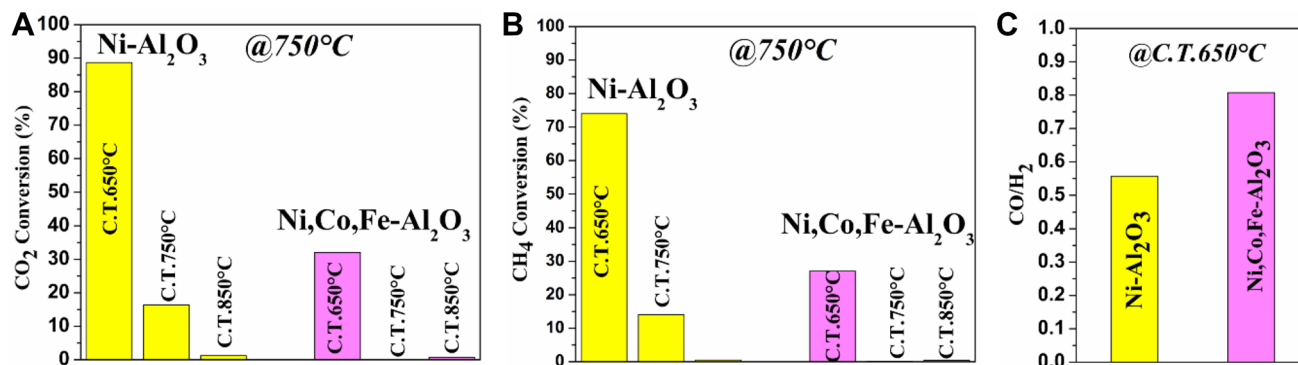

Fig. 5 Catalytic test measurements results: **A** CO$_2$ conversion of Ni–Al$_2$O$_3$ and Ni,Co,Fe–Al$_2$O$_3$ catalysts calcined at different temperatures, **B** CH$_4$ conversion of the catalysts and **C** CO/H$_2$ ratio of Ni–Al$_2$O$_3$ and Ni,Co,Fe–Al$_2$O$_3$ catalysts at 750 °C
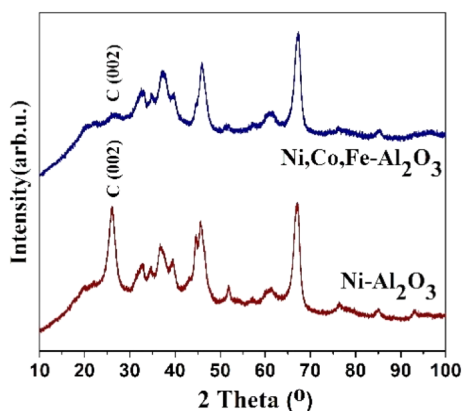
Fig. 6 XRD of spent Ni-Al$_2$O$_3$ and Ni, Co, Fe–Al$_2$O$_3$ catalysts calcined at 650 °C

sites, which are the most active sites for the reforming reaction, are where a fraction of the potassium migrates from the support to the nickel surface. As a consequence, conversion

rates of reactants are reduced when there is a low potassium content [14]. (Fig. 7, 8).

DRIFTS spectra were collected at elevated temperatures over Ni,Co,Fe–Al$_2$O$_3$ and K/Ni,Co,Fe–Al$_2$O$_3$ calcined at 650 °C in order to establish surface adsorbed species formed during the DRM reaction and derive the influence of Potassium onto the catalytic performance (Fig. 9). The assignment of IR bands was based on the previously reported vibrational fingerprints of relevant surface species.

No additional peaks evolved or seized with the Potassium addition. The main difference which can be spotted is the significant reduction in the intensity of the 1650 cm^{-1} IR band. The peaks at 1645–1650 cm^{-1} and ~1345 cm^{-1} may be assigned to the asymmetric and symmetric νCOO− vibration of bicarbonate anions, correspondingly [34]. The formation of bicarbonate species usually originates from the interaction between CO$_2$ molecules and the surface hydroxyl groups of the alumina support [35].

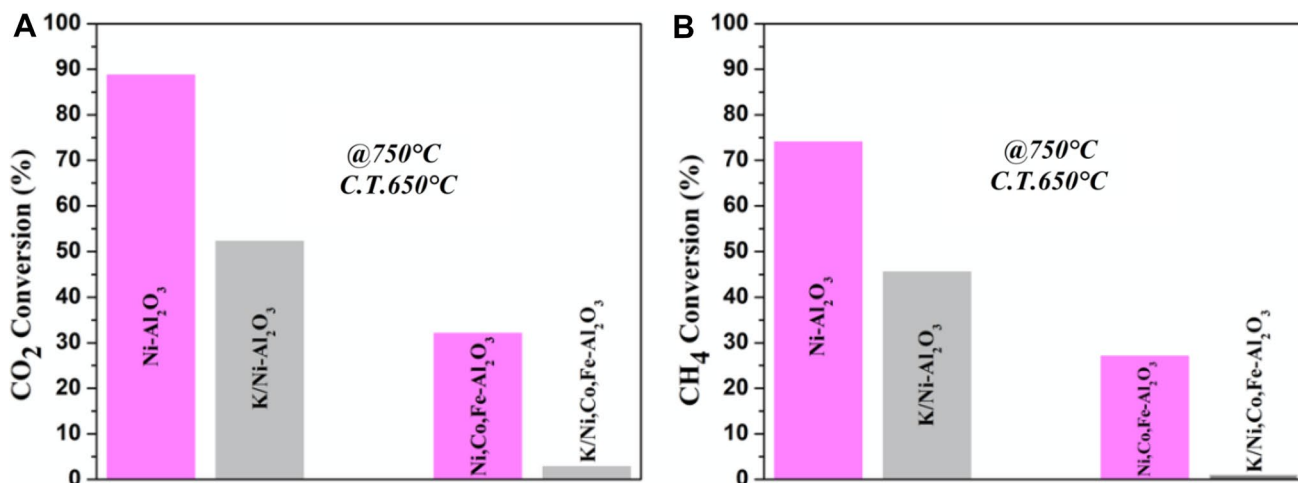From 773 K bicarbonate species are transformed to the formate species at 2600 cm^{-1} (not shown) and ~1588 cm^{-1}

Fig. 7 Catalytic test measurements results: **A** CO2 conversion, **B** CH4 conversion of Ni–Al$_2$O$_3$, K/Ni–Al$_2$O$_3$, Ni, Co,Fe–Al$_2$O$_3$ and K/Ni,Co,Fe–Al$_2$O$_3$ catalysts calcined at 650 °C temperatures (reaction temperature:750 °C).
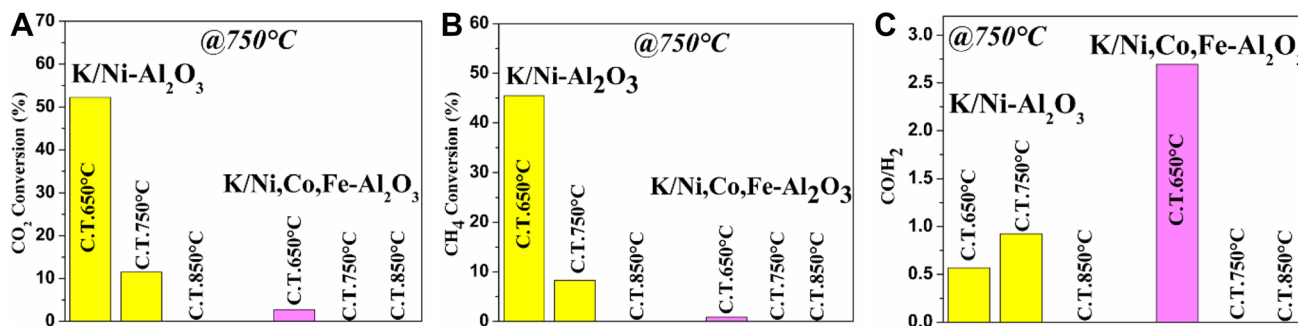
Fig. 8 Catalytic test measurements results: **A** CO$_2$ conversion, **B** CH$_4$ conversion and **C** CO/H$_2$ ratio of K/Ni–Al$_2$O$_3$ and K/Ni,Co,Fe–Al$_2$O$_3$ catalysts calcined at different temperatures at 750 °C
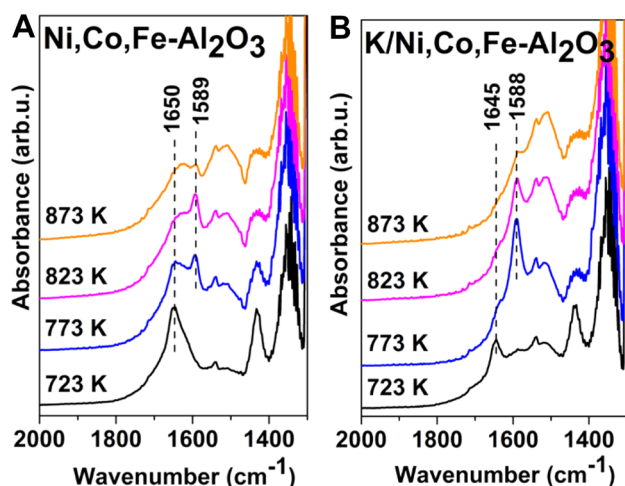
Fig. 9 DRIFT spectra collected at elevated temperatures during DRM reaction over: **A** Ni,Co,Fe–Al$_2$O$_3$ and **B** K/Ni,Co,Fe–Al$_2$O$_3$ catalysts calcined at 650 °C

[36, 37]. The decomposition of formate, which is favored at high temperatures, generates CO which then desorbs from the surface. Gaseous H$_2$ is formed by coupling of the surface hydrogen atoms, produced during the dehydrogenation of methane on the metallic surfaces [33].

The bands in the spectral region from ~1300 to 1550 cm^{-1} correspond to the different forms of adsorbed carbonate species [38].

The Potassium-promoted sample shows considerably lower intensity and broadened bicarbonate feature (Fig. 9B), which is probably due to the interaction of Potassium with the alumina hydroxyl groups by the partial K$^+$ for H$^+$ cationic exchange [39] This might be the reason for the deterioration in the catalytic performance with the addition of Potassium.

4 Conclusion

In this study, Ni–Al$_2$O$_3$, K/Ni–Al$_2$O$_3$, Ni, Co, Fe–Al$_2$O$_3$, and K/Ni, Co, Fe–Al$_2$O$_3$ catalysts were prepared at 3 different calcination temperatures: 650,750 and 850 °C. Trimetallic catalysts displayed a more favorable CO/H$_2$ ratio and significantly better coke resistance compared to the reference Ni–Al$_2$O$_3$ catalyst at the expense of lower catalytic conversion. The results demonstrated that alloying of 3 metals at 650 °C calcination temperature can be applied to produce syngas which subsequently can be directly used for the Fischer–Tropsch synthesis. In addition, using K as a promoter to lessen coke deposition resulted in a decrease in the conversion rates of reactants.

Declarations

Conflict of interest There are no conflicts to declare. The authors declare no competing financial interest.

References

1. Sápi A, Rajkumar T, Ábel M, Efremova A, Grósz A, Gyuris A et al (2019) Noble-metal-free and Pt nanoparticles-loaded, mesoporous oxides as efficient catalysts for CO$_2$ hydrogenation and dry reforming with methane. J CO2 Util 32:106–18
2. Teh LP, Setiabudi HD, Timmiati SN, Aziz MAA, Annuar NHR, Ruslan NN (2021) Recent progress in ceria-based catalysts for the dry reforming of methane: a review. Chem Eng Sci 12:242
3. Owgi AHK, Jalil AA, Hussain I, Hassan NS, Hambali HU, Siang TJ et al (2021) Catalytic systems for enhanced carbon dioxide reforming of methane: a review. Environ Chem Lett 19(3):2157–83
4. Abasaeed AE, Al-Fatesh AS, Naeem MA, Ibrahim AA, Fakeeha AH (2015) Catalytic performance of CeO$_2$ and ZrO$_2$ supported Co catalysts for hydrogen production via dry reforming of methane. Int J Hydrogen Energy 40(21):6818–6826
5. Arora S, Prasad R (2016) An overview on dry reforming of methane: strategies to reduce carbonaceous deactivation of catalysts. RSC Adv 6(110):108668–88
6. Gao X, Ge Z, Zhu G, Wang Z, Ashok J, Kawi S (2021) Anti-coking and anti-sintering Ni/Al$_2$O$_3$ catalysts in the dry reforming of methane: recent progress and prospects. Catalysts 11(8):1003
7. Bu K, Deng J, Zhang X, Kuboon S, Yan T, Li H et al (2020) Promotional effects of B-terminated defective edges of Ni/boron nitride catalysts for coking- and sintering-resistant dry reforming of methane. Appl Catal B 15:267
8. Ali S, Khader MM, Almarri MJ, Abdelmoneim AG (2020) Ni-based nano-catalysts for the dry reforming of methane. Catal Today 1(343):26–37

9. Yan X, Hu T, Liu P, Li S, Zhao B, Zhang Q et al (2019) Highly efficient and stable Ni/CeO$_2$-SiO$_2$ catalyst for dry reforming of methane: Effect of interfacial structure of Ni/CeO$_2$ on SiO$_2$. Appl Catal B 5(246):221–231

10. Ian Z, Das S, Ing M, Wai H, Hongmanorom P, Kawi S (2017) A review on bimetallic nickel-based catalysts for CO$_2$ reforming of methane. ChemPhysChem 12(22):3117–3134

11. Horváth A, Németh M, Beck A, Maróti B, Sáfrán G, Pantaleo G et al (2021) Strong impact of indium promoter on Ni/Al$_2$O$_3$ and Ni/CeO$_2$-Al$_2$O$_3$ catalysts used in dry reforming of methane. Appl Catal A Gen 5:621

12. Yan X, Xi-hua D, Jing L, Peng W, Jie Z, Feng-juan G et al (2019) Foundation items: Supported by the National Natural Science Foundation of China (21703194), the Natural Science Foundation of Jiangsu Province (BK20171168, BK20171169). J Fuel Chem Technol 47(2):199–208

13. Tsiotsias AI, Charisiou ND, Yentekakis I v, Goula MA (2020) The role of alkali and alkaline earth metals in the Co$_2$ methanation reaction and the combined capture and methanation of Co$_2$. Catalysts 10(7):812

14. Juan-Juan J, Román-Martínez MC, Illán-Gómez MJ (2006) Effect of potassium content in the activity of K-promoted Ni/Al$_2$O$_3$ catalysts for the dry reforming of methane. Appl Catal A Gen 301(1):9–15

15. Franz R, Pinto D, Uslamin EA, Urakawa A, Pidko EA (2021) Impact of promoter addition on the regeneration of Ni/Al$_2$O$_3$ Dry reforming catalysts. ChemCatChem 13(23):5034–5046

16. Jawad A, Rezaei F, Rownaghi AA (2020) Highly efficient Pt/Mo-Fe/Ni-based Al$_2$O$_3$–CeO$_2$ catalysts for dry reforming of methane. Catal Today 15(350):80–90

17. Theofanidis SA, Galvita V v, Poelman H, Marin GB (2015) Enhanced carbon-resistant dry reforming Fe–Ni catalyst: role of Fe. ACS Catal 5(5):3028–39

18. Lyu L, Shengene M, Ma Q, Sun J, Gao X, Fan H et al (2022) Synergy of macro-meso bimodal pore and Ni-Co alloy for enhanced stability in dry reforming of methane. Fuel 15:310

19. Joo S, Kim K, Kwon O, Oh J, Kim HJ, Zhang L et al (2021) Enhancing thermocatalytic activities by upshifting the d-band center of exsolved Co-Ni-Fe ternary alloy nanoparticles for the dry reforming of methane. Angew Chem—Int Edition 60(29):15912–15919

20. Al-Fatesh AS, Abu-Dahrieh JK, Atia H, Armbruster U, Ibrahim AA, Khan WU et al (2019) Effect of pre-treatment and calcination temperature on Al$_2$O$_3$–ZrO$_2$ supported Ni–Co catalysts for dry reforming of methane. Int J Hydrogen Energy 44(39):21546–21558

21. Le TA, Kim TW, Lee SH, Park ED (2017) CO and CO$_2$ methanation over Ni catalysts supported on alumina with different crystalline phases. Korean J Chem Eng 34(12):3085–3091

22. Garbarino G, Kowalik P, Riani P, Antoniak-Jurak K, Pieta P, Lewalska-Graczyk A et al (2021) Improvement of Ni/Al$_2$O$_3$ catalysts for low-temperature CO$_2$ methanation by vanadium and calcium oxide addition. Ind Eng Chem Res 60(18):6554–6564

23. Zhou L, Li L, Wei N, Li J, Basset JM. Effect of NiAl$_2$O$_4$ Formation on Ni/Al$_2$O$_3$ Stability During Dry Reforming of Methane [Internet]. Available from: www.chemcatchem.org

24. Park KS, Jeong MH, Bae JW (2020) Synergy effects of cobalt oxides on Ni/Co-embedded Al$_2$O$_3$ for hydrogen-rich syngas production by steam reforming of propane. Catalysts 10(4):461

25. Gangwar J, Gupta BK, Kumar P, Tripathi SK, Srivastava AK (2014) Time-resolved and photoluminescence spectroscopy of θ-Al$_2$O$_3$ nanowires for promising fast optical sensor applications. Dalton Trans 43(45):17034–17043

26. Urbonavicius M, Varnagiris S, Pranevicius L, Milcius D (2020) Production of gamma alumina using plasma-treated aluminum and water reaction byproducts. Materials 13(6):1300

27. Jastrzębska I, Stępień J, Żukrowski J, Szczerba J. Stabilization of hercynite structure at elevated temperatures by Mg substitution [Internet]. Available from: https://ssrn.com/abstract=4074556

28. You X, Wang X, Ma Y, Liu J, Liu W, Xu X et al (2014) Ni-Co/Al$_2$O$_3$ bimetallic catalysts for CH4 steam reforming: elucidating the role of Co for improving coke resistance. ChemCatChem 6(12):3377–3386

29. Aramouni NAK, Zeaiter J, Kwapinski W, Leahy JJ, Ahmad MN (2021) Trimetallic Ni-Co-Ru catalyst for the dry reforming of methane: Effect of the Ni/Co ratio and the calcination temperature. Fuel 15:300

30. Franz R, Franz R, Kühlewind T, Shterk G, Abou-Hamad E, Parastaev A et al (2020) Impact of small promoter amounts on coke structure in dry reforming of methane over Ni/ZrO$_2$. Catal Sci Technol 10(12):3965–3974

31. Kim WY, Lee YH, Park H, Choi YH, Lee MH, Lee JS (2016) Coke tolerance of Ni/Al$_2$O$_3$ nanosheet catalyst for dry reforming of methane. Catal Sci Technol 6(7):2060–2064

32. Jiao X, Qiu Y, Zhang L, Zhang X (2017) Comparison of the characteristic properties of reduced graphene oxides synthesized from natural graphites with different graphitization degrees. RSC Adv 7(82):52337–52344

33. Wysocka I, Mielewczyk-Gryń A, Łapiński M, Cieślik B, Rogala A (2021) Effect of small quantities of potassium promoter and steam on the catalytic properties of nickel catalysts in dry/combined methane reforming. Int J Hydrogen Energy 46(5):3847–3864

34. Foo GS, Lee JJ, Chen CH, Hayes SE, Sievers C, Jones CW (2017) Elucidation of surface species through in Situ FTIR spectroscopy of carbon dioxide adsorption on amine-grafted SBA-15. Chemsuschem 10(1):266–276

35. Falbo L, Visconti CG, Lietti L, Szanyi J (2019) The effect of CO on CO$_2$ methanation over Ru/Al$_2$O$_3$ catalysts: a combined steady-state reactivity and transient DRIFT spectroscopy study. Appl Catal B 5:256

36. László B, Baán K, Oszkó A, Erdőhelyi A, Kiss J, Kónya Z (2018) Hydrogen evolution in the photocatalytic reaction between methane and water in the presence of CO2 on titanate and titania supported Rh and Au catalysts. Top Catal 61(9–11):875–888

37. Wang X, Shi H, Kwak JH, Szanyi J (2015) Mechanism of CO2 hydrogenation on Pd/Al2O3 catalysts: kinetics and transient DRIFTS-MS studies. ACS Catal 5(11):6337–6349

38. Efremova A, Rajkumar T, Szamosvölgyi Á, Sápi A, Baán K, Szenti I et al (2021) Complexity of a Co$_3$O$_4$ system under ambient-pressure CO$_2$ Methanation: influence of bulk and surface properties on the catalytic performance. J Phys Chem C 125(13):7130–7141

39. Montanari T, Matarrese R, Artioli N, Busca G (2011) FT-IR study of the surface redox states on platinum-potassium-alumina catalysts. Appl Catal B 105(1–2):15–23